Proceedings SIMS X 1995
in press

PRESENT STATUS OF LASER POSTIONIZATION ANALYSES

H. F. Arlinghaus, T.J. Whitaker, C. F. Joyner, P. Kwoka, B. Jacobson[1], and J. Tower[2]

Atom Sciences, Inc., 114 Ridgeway Center, Oak Ridge, TN 37830, USA
[1] Oak Ridge National Laboratory, Oak Ridge, TN 37831, USA
[2] Loral Infrared & Imaging Systems, Lexington, MA 02173, USA

Secondary Ion Mass Spectrometry (SIMS) is one of the most versatile, and in recent years among the most frequently used techniques for surface and depth profile analysis. SIMS, however, has several limitations, some inherent in secondary ion formation, some due to the physics of ion beams, and some due to the nature of sputtering. Sputtering produces predominantly neutral atoms; the secondary ion yield is typically between 10^{-4} to 10^{-7} for most of the elements in the periodic table. This leads to a serious sensitivity limitation when extremely small volumes must be probed, or when high lateral and depth resolution analyses are needed. Another problem stems from the fact that secondary ion yield can vary by many orders of magnitude as a function of surface contamination and matrix composition making quantitation very difficult. Quantitation can also be jeopardized by interferences from molecules, molecular fragments, and isotopes of other elements having the same mass as the analyte. Very high mass resolution can reject such interferences but only at the expense of detection sensitivity.

To improve sensitivity and quantitation, several postionization methods have been developed. These techniques decouple the sputtering and ionization processes by ionizing the sputtered neutral atoms after emission from the sample surface. In secondary neutral mass spectrometry (SNMS) [1-4], the sputtered neutrals are ionized in a plasma or by electron-impact ionization. While the secondary ion yield can vary widely with the surface composition, this is not true of the neutral yield. For example, a variation in the secondary ion yield over three orders of magnitude (10^{-4} to 10^{-7}) produces less than a 1% change in the yield of neutrals. As a result, SNMS has much smaller matrix effects than SIMS, but is less sensitive due to the inefficient ionization process, and still suffers from isobaric interferences from molecular fragments, clusters, and/or molecules formed in the sputtering process or in the plasma. Surface analysis by laser ionization (SALI) [1, 5-7] and femtosecond postionization [8,9] have been used to improve the ionization efficiency (as compared to SNMS) while retaining the advantages of probing the neutral component. In both techniques, an intense laser beam is used to nonselectively ionize all the elements and molecules within the volume intersected by the laser beam. With sufficient power densities, it is possible to saturate the ionization process. For SALI, adequate power densities are typically achieved only in a small volume at the focus of the laser beam. This reduces sensitivity and leads to problems with quantitation due to the differences in effective

ionization volume for different elements. Both SALI and femtosecond postionization techniques provide rapid, multi-element and molecular survey measurements with improved ionization efficiency over SNMS, but like SNMS, they suffer from isobaric interferences. While less susceptible to matrix effects than SIMS, these techniques are not completely free of matrix effects because changes in the sputter yield (as a function of matrix) can cause quantitation errors. This can be corrected by using standards or determining the various sputter yields. Recombination effects (especially in SNMS) and incomplete atomization are other possible sources of matrix effects for these techniques.

Sputter-Initiated Resonance Ionization Microprobe (SIRIMP) [10-15] has almost all the advantages of SIMS, SNMS, and SALI, but has the additional advantage of using a resonance laser ionization process which selectively and efficiently ionizes the desired elemental species over a relatively large volume. Like SNMS and SALI, SIRIMP probes the neutral component of the sputtered material and therefore has reduced matrix dependence. In addition, for over 80% of the elements in the periodic table, SIRIMP has almost unity ionization efficiency over a large volume so the overall efficiency is greater than SALI. Quantitation is also made simpler because the unsaturated volume (where ionization is incomplete) is insignificant compared to the saturated volume. This leads to consistently high sensitivity and greater accuracy in the SIRIMP measurements. Unlike SIMS, SNMS, and SALI, the SIRIMP ionization process is selective, thus producing fewer isobaric and molecular interferences. This improves the accuracy of the data and simplifies its interpretation without requiring very high resolution (expensive) mass spectrometry. The main drawbacks accompanying this immunity to interference are that only one element is analyzed at a time and that low-repetition rate pulsed lasers impose a low duty cycle. Multiple lasers can be used permit analysis of multiple elements but this is limited practically to two or three elements. Advances in diode-pumped Nd:YAG lasers and optical parametric oscillators (OPO's) will allow increase of the repetition rate from currently available 30-100 Hz models to 600 Hz or higher [16].

In SIRIMP experiments, the sample is bombarded with a finely focused pulsed primary ion beam. During the time the primary ion pulse is striking the target, voltages on the extraction electrodes are set so that electric fields retard positive secondary ions. After the primary ion pulse, the voltages are switched so that ions formed by laser resonance ionization of the neutral particles in the sputtered cloud have significantly different energy than the secondary ions formed in the sputtering process. Ions are analyzed by a time-of-flight mass spectrometer with an electrostatic energy analyzer which discriminates against the secondary ions. The TOF allows all isotopes of the analyte element to be simultaneously measured in each laser shot. Mass spectrometer requirements are reduced to resolving neighboring isotopes of a single element.

SIRIMP imaging is achieved by either scanning the ion beam over the sample or by translating the sample under a fixed ion beam. If a liquid ion gun is used for sputtering, nanoanalysis down to 50 nm can be achieved. Charge compensation for insulator analyses is possible using pulsed low energy electrons, which are introduced during the time interval between sputtering pulses. SIRIMP depth profiles can be

obtained by scanning the sample with a continuous ion beam and taking data with a pulsed ion beam in the center of the crater after each raster frame. In SIRIMP, as in other microprobe techniques, the combination of 2-d imaging with depth profile capabilities allows visualization of three-dimensional distribution of elements. However, the extremely high overall efficiency of SIRIMP (typically 3% to 8% useful yield for most elements) permits measurement of low concentrations of analytes in much smaller volumes, thus enabling higher lateral and depth resolution in these 3d visualizations. This capability could greatly contribute to the study of dopant and contaminant distributions in semiconductor devices.

The efficiency of SIRIMP is due to several factors. First of all, SIRIMP probes the neutral component of the sputtered material (similar to SNMS and SALI), and neutrals typically make up over 99% of most sputtered species. Secondly, the resonant ionization (RI) process is very efficient because the intensity of modern pulsed tunable lasers is sufficient to saturate all steps of RI over large volumes (focussing is not required). This assures near unit probability of ionizing all ground-state atoms of the selected element that are in the volume intersected by the RI laser beams. With careful spatial and temporal overlap of the laser beams with the cloud of desorbed material, useful yields (atoms detected/atoms sputtered) between 3% to 8% are obtained, giving sub-parts-per billion detection limits [12-14].

Both the efficiency and selectivity of resonance ionization stem from the resonance excitation step(s). Cross-sections for resonant excitation are orders of magnitude greater than those for nonresonant excitation and therefore relatively low-power lasers produce efficient excitation without focussing. Transition wavelengths for most elements are separated from those of other elements by values greater than the bandwidth of commercial lasers. Therefore, when the laser is tuned to resonance with the analyte element, it is typically far off resonance with any potentially interfering elements. This is the reason that RI is extremely selective. We have previously demonstrated that ionization efficiency for the selected element can be as much as 10^9 times higher than for the other elements in the sample. Molecular interferences can be a problem because their broad absorption bands may overlap the resonance, but the effect is quite small because the oscillator strength is spread out over the entire vibrational/rotational band, and the effect becomes negligible in most cases when a double resonance scheme is used.

RI selectivity helps simplify interpretation of data by reducing or eliminating interferences and it helps maintain signal linearity by reducing space charge effects that would otherwise be present due to ionization of major constituents of the sample. The use of two resonance steps generally offers better selectivity than single-resonance schemes. Figure 1 shows generic single-resonance, double-resonance, and non-resonance schemes. Scheme (a) in this figure shows a simple single-resonance scheme. This is the simplest but not necessarily the most desirable scheme. Photoionization cross-sections are much lower than those for resonance steps and therefore the photoionization laser intensity must be proportionally higher in order to efficiently ionize the atoms. High-intensity visible or UV laser beams can cause nonlinear ionization of interfering species but this is seldom a problem with high-intensity IR beams. Therefore, whenever selectivity is an issue, it is better to use IR

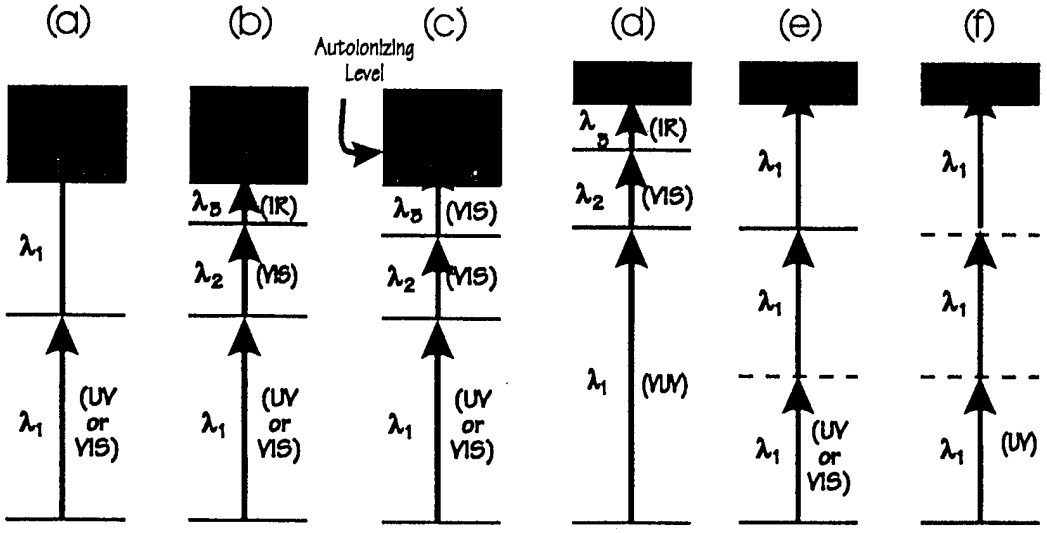

Figure 1. Different implementations of the resonance ionization concept. Scheme (b) and (c) give the best selectivity and are applicable to over 85% of the elements.

wavelengths for the photoionization step. Scheme (b) is the most versatile of the schemes shown and it gives the best performance. Only H, He, C, N, O, F, Ne, P, S, Cl, Ar, Br, Kr, I, Xe, and Rn cannot be analyzed using Scheme (b) with commercial laser systems and frequency upconversion in nonlinear crystals. RI Scheme (c) can be used when autoionizing structure exists in the ionization continuum. The cross-section for autoionization is significantly larger than for normal photoionization and therefore the intensity of the ionizing laser can be reduced. This allows the use of visible wavelengths without extensive nonlinear ionization of interfering species. Scheme (d) is used when even the lowest-energy excited states of the analyte element require vacuum UV wavelengths. It differs from Scheme (b) only in the experimental method used to generate the wavelength for the first transition. For wavelengths below about 195 nm, either four-wave mixing or anti-Stokes Raman must be used. This makes Scheme (d) the most experimentally complex of the resonance ionization schemes. We have used this technique in our laboratory to measure the amount of ^{81}Kr (a radioactive isotope with approximately 1 part in 10^{18} natural abundance in the atmosphere) in a water sample after several isotope enrichment steps [17]. Scheme (e) is generally used when the energy of the excited state structure is too high for Schemes (a), (b), or (c) and the researcher does not wish to go to the experimental complexity of Scheme (d). Examples are C, N, O, P, S, Cl, Br, Kr, I, and Xe. The two-photon transition used in Scheme (e) is a second-order process and therefore its cross-section is quite low compared to the one-photon transitions described in the other schemes. This means that high-intensity light is needed, and focussing of the laser beam is generally required. In fact, the intensity of the light needed for efficient two-photon excitation is usually sufficient to ionize the excited state and so Scheme (e) often requires only a single wavelength. This experimental simplicity is counterbalanced by the fact that the high-intensity light can cause nonlinear processes, including multiphoton

ionization, to occur in many other species, leading to interferences. This problem is even greater in nonresonant ionization, shown in Scheme (f).

Isotope shifts for most elements are small in comparison to the bandwidth of the pulsed lasers used in RI experiments (the pulsed lasers used in the authors' laboratory have 7 - 12 GHz bandwidth), and thus all the isotopes of the analyte will be essentially resonant with the RI laser. In this case, isotopic analysis is achieved with a mass spectrometer (this is often called Resonance Ionization Mass Spectrometry, or RIMS). Time-of-flight mass spectrometers are especially well-suited for isotopic analysis of ions produced by pulsed RI lasers because all the ions are detected on each pulse. One might expect that as long as the laser bandwidth is wider than the isotopic splitting, all isotopes will be ionized with equal efficiency. This has been shown to not be the case in several experiments where odd-even isotope anomalies have been reported [18]. Lambropoulos has explained in a series of papers [19] that this phenomenon is due to the coupling between hyperfine states of isotopes with nonzero nuclear spin. The magnitude of this effect is dependent on several factors but it is possible to obtain reproducible results if all these factors are controlled, and therefore it is practical to use standards to calibrate the odd-even isotope effect for a particular RI system.

The SIRIMP instrument in the authors' lab consists of a versatile microfocus ion gun (incident angle = 60° from normal), a sputtering ion gun, an FEI liquid metal ion gun, a pulsed flood electron gun, a 30 Hz RI laser system consisting of a pulsed Nd:YAG laser pumping two dye lasers, a computer-controlled high-resolution sample manipulator on which samples can be cooled to 110 K, a video and electron imaging system, a vacuum lock for sample introduction, and a TOF mass spectrometer. Two of the ion guns have high-purity Mo apertures and Wien filters to prevent contamination of the sample.

Figure 2 shows Cu depth profiles obtained from silicon and 0.8 μm silicon oxide on silicon samples. For this experiment, half a silicon wafer and half a silicon oxide wafer were simultaneously implanted with $5x10^{14}$ ^{63}Cu atoms/cm^2 at 150 keV. This sample was made to (a) determine the SIRIMP Cu sensitivity factor and (b) investigate how quantitative and matrix independent the SIRIMP technique is. For analysis, both samples were cooled to 107K to reduce migration effects, and depth profiles were taken under the same experimental conditions. The integrated Cu signal for both samples, i.e. the Cu sensitivity factor for Cu in silicon and

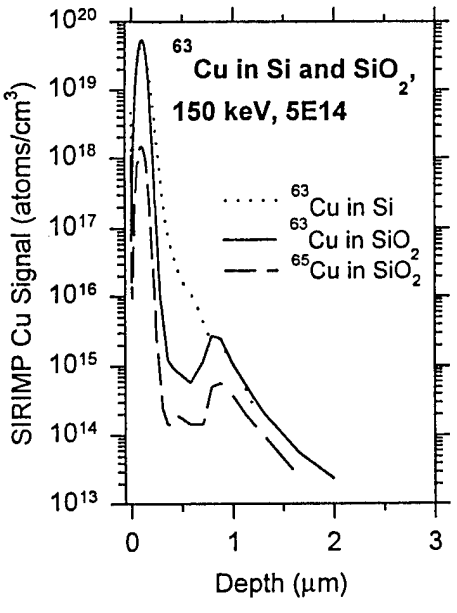

Figure 2. Depth profile of ^{63}Cu in Si and both ^{63}Cu and ^{65}Cu in SiO_2.

Cu in silicon oxide was almost the same (less than a 3% difference which is probably due to the differences in sputter yield), demonstrating the matrix independence and the quantitation accuracy possible with SIRIMP. At the SiO_2/Si interface, a higher Cu concentration was observed. The isotopic ratio at this pile-up near the interface and below is closer to that of natural copper, indicating that the sample was contaminated with Cu when the oxide was grown. The measured Cu profile for silicon oxide could be fitted quite well with TRIM89, while the trailing edge of the Cu profile in silicon was broadened in comparison to the calculated TRIM89 curve[20]. This is probably due to channeling effects which occur in crystalline silicon but not in amorphous silicon oxide.

Figure 3 shows a photomicrograph of Te inclusions in CdZnTe and a SIRIMP image of the copper concentration around the inclusions. It is clear from the images that the copper concentration is 5-25 times greater in the Te inclusion than in the surrounding CdZnTe matrix. These data support the theory that the copper preferentially migrates to Te second phase regions inside the CdZnTe matrix. Similar SIRIMP results were recently obtained for 10-30 μm size Te and Cd inclusions in HgCdTe samples[21].

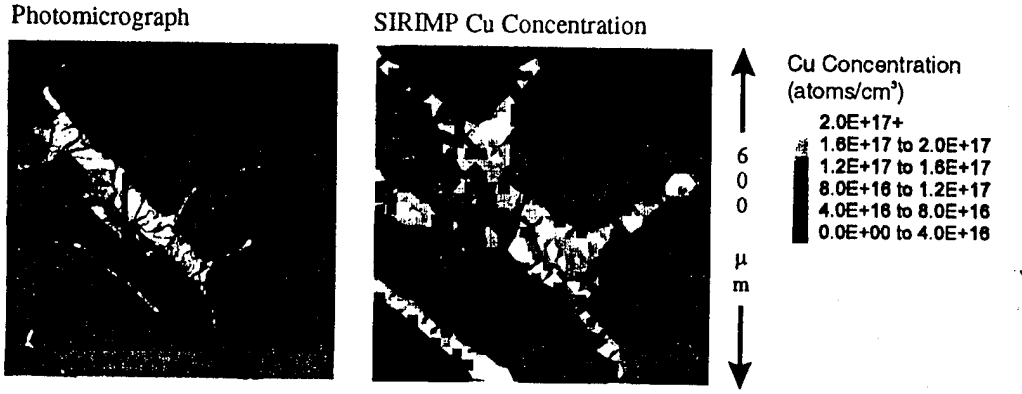

Figure 3. Optical micrograph of Te inclusions in CdZnTe and SIRIS image of Cu concentrations of a region around the inclusion. The SIRIS scale is in atoms/cm^3.

SIRIMP can be also applied to detect Sn-labeled DNA at positively hybridized and unhybridized sites on a Form I and Form II DNA sequencing matrices which can be used for genetic disease and cancer diagnostics. Form I sequencing by hybridization (SBH) is a method where the large genomic DNA is attached to the solid surface, such as a nylon membrane, and the labeled (in our case with enriched isotopes) oligonucleotides of known sequence are allowed to hybridize. Form II SBH involves binding a small (typically 18 - 20-mer) oligonucleotide to a chip. The chip might be glass, silicon, platinum or gold. By the process of polymerase chain reaction, fragments of the genomic DNA are produced with an attached label. The size of the fragment can vary from a few dozen to several hundred or several thousand nucleotides. Both methods have advantages and disadvantages. It is easier to bind large DNA molecules rather than small ones to nylon. Conversely, only small molecules can be bound to silicon or noble metal surfaces, at this time.

Figure 4 shows a SIRIMP image of ^{118}Sn obtained from a SBH Form II matrix. For this experiment two different 17-mer oligonucleotides were bound to platinum circles on a silicon wafer at a total of six locations (three locations each). Then enriched ^{118}Sn-labeled DNA, which was completely complimentary to one of these oligonucleotides, and noncomplimentary to the other, was hybridized to the chip. After the hybridization, the sample was washed to remove unhybridized probes. The image shows three peaks at the complementary DNA sites. The discrimination between hybridized and unhybridized sites is better than 100. A single point on the top center spot was analyzed twice before the full image was taken, leading in a slight reduction of the signal. Similar data have been obtained for a Form I experiment on nylon.

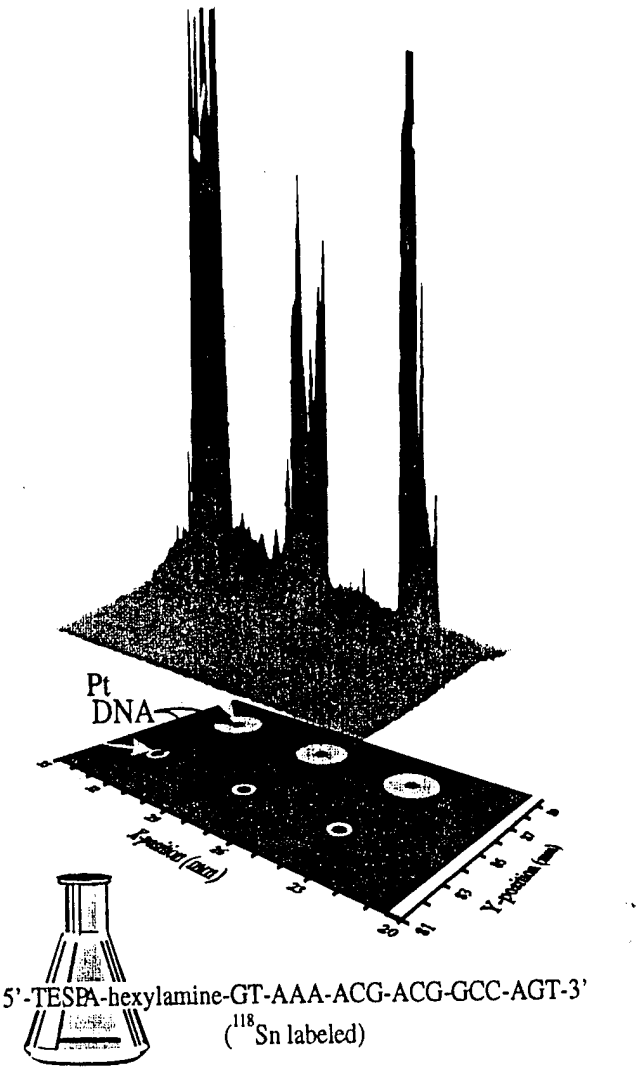

Figure 4. SIRIS ^{118}Sn image of Sn-labelled DNA hybridized to 6 oligonucleotide spots; 3 complimentary and 3 noncomplimentary.

Analytical requirements in a number of fields are beginning to exceed conventional capabilities. As this trend continues, the use of postionization and, in particular, resonance postionization (SIRIMP) will become a necessary tool for a number of applications.

This work was partly supported by the Advance Research Projects Agency (Contract DAAH01-92-C-R372), the National Institutes of Health (Contracts 1 R43 MH 52938-01 and 1 R43 CA66525-01), and the IRMP program (Contract # MDA972-91-C-0046) from ARPA, We thank K. Beattie, Houston Advanced Research Center, and D. Simons and P. Roitman, National Institute for Standards and Technology, for samples.

REFERENCES

1. See articles in "Secondary Ion Mass Spectrometry - SIMS VIII," eds. A. Benninghoven, K.T.F. Janssen, J. Tümpner, and H.W. Werner, John Wiley and Sons (1992) and previous proceedings.
2. H. Oechsner, in "Thin Film and Depth Profile Analysis", ed. H. Oechsner, Springer-Verlag, 1984.
3. H. Gnaser, J. Fleischhauer, and W.O. Hofer, *Appl. Phys.* **A37**, 211 (1985).
4. D. Lipinsky, R. Jede, O. Ganschow, and A. Benninghoven, *J. Vac. Sci. Technol.* **A3**, 2007 (1985).
5. C.H. Becker and K.T. Gillen, *Anal. Chem.* **56**, 1671 (1984).
6. C.H. Becker, *J. Vac. Sci. Technol.* **A5**, 1181 (1987).
7. J.B. Pallix, C.H. Becker, and N. Newman, *J. Vac. Sci. Technol.* **A6**, 1049 (1988).
8. N. Winograd, private communication.
9. A. Benninghoven, B. Hagenhoff, and E. Niehuis, *Anal. Chem.* **65**, 630A (1993).
10. N. Thonnard, J.E. Parks, R.D. Willis, L.J. Moore, and H.F. Arlinghaus, *Surf. Interface Anal.* **14**, 751 (1989).
11. H.F. Arlinghaus, M.T. Spaar, and N. Thonnard, *J. Vac. Sci. Technol.* **A8**, 2318 (1990).
12. H.F. Arlinghaus, M.T. Spaar, and N. Thonnard, A.W. McMahon, T. Tanigaki, H. Shichi, P.H. Holloway, *J. Vac. Sci. Technol.* **A11**, 2317 (1993).
13. D.L. Pappas, D.M. Hrubowchak, M.H. Ervin, and N. Winograd, *Science* **243**, 64 (1989).
14. M.J. Pellin, C.E. Young, W.F. Calaway, J.E. Whitten, D.M. Gruen, J.B. Blum, I.D. Hutcheon and G.J. Wasserburg, *Phil. Trans. R. Soc. Lond.* **A 333**, 133 (1990).
15. S.W. Downey, A.B. Emerson and R.F. Kopf in "Resonance Ionization Spectroscopy 1990, eds. J.E. Parks and N. Omenetto, Inst. Phys. Conf. Ser. No **114**, p. 401 (1990).
16. J.J. Ewing, Aculight, Bellevue, WA, private communication.
17. N. Thonnard, R.D. Willis, M.C. Wright, W.A. Davis, and B.E. Lehman, "Resonance ionization spectroscopy and the detection of ^{81}Kr", *Nucl. Instr. and Meth. in Phys. Res. B* **29** 398-406 (1987).
18. W.M. Fairbank, Jr., M.T. Spaar, J.E. Parks, and J.M.R. Hutchinson, "Anomalous odd- to even-mass isotope ratios in resonance ionization with broad-band lasers", *Phys. Rev. A* **40**(4) 2195-2198 (1989).
19. P. Lambropoulos and A. Lyras, Resonance Ionization Spectroscopy, edited by T.B. Lucatorto and J. Parks, IOP, Bristol, 1-6 (1989).
20. H.F. Arlinghaus and C.J. Joyner, J. Vac. Sci. Technol. **B14(1)**, 1996, in press.
21. H.F. Arlinghaus, C.F. Joyner, J. Tower, and S. Sen, elsewhere in this proceedings.